Statistical Image Analysis of Electron Micrographs of Ribosomal Subunits

Harauz, George; Boekema, Egbert; Heel, Marin van

Published in:
Default journal

Publication date:
1988

vation of particles from negatively stained preparations can be assessed and also by revealing for the first time the structure of the native ribosomal particle as it is investigated by other, non-EM techniques.

Acknowledgments

This work was supported, in part, by a grant of the National Institute of Health 1RO1 GM 29169 and a shared instrumentation grant of the National Science Foundation 831345.

[2] Statistical Image Analysis of Electron Micrographs of Ribosomal Subunits

By GEORGE HARAUZ, EGBERT BOEKEMA, and MARIN VAN HEEL

Electron microscopy in combination with computer-image analysis represents a very direct method for determining the structure of biological macromolecules. Crystallographic techniques allow the determination of structure to higher resolution; however, for large macromolecular assemblies such as ribosomes, sufficiently large and perfect crystals are extremely difficult to obtain. Thus, electron microscopy of individual biological macromolecules has been developing as an alternative or complement to the traditional crystallographic approaches.

Ribosomal structure has been extensively probed by electron microscopy.[1-7] However, since electron images are very noisy, agreement on even low-resolution models of ribosome structure has been slow in developing.[8] The visual interpretation of micrographs is a subjective process that varies from observer to observer, especially concerning those details at the limits of the attainable resolution. Our research has focused on establishing a precise methodology based on computerized image analysis and pattern recognition to enhance the visibility of statistically signifi-

[1] H. G. Wittmann, *Annu. Rev. Biochem.* **52,** 35 (1983).
[2] G. Stöffler and M. Stöffler-Meilicke, *Annu. Rev. Biophys. Bioeng.* **13,** 303 (1984).
[3] V. D. Vasiliev, O. M. Selivanova, and S. N. Ryazantsev, *J. Mol. Biol.* **1711,** 561 (1983).
[4] A. P. Korn, D. Elson, and P. Spitnik-Elson, *Eur. J. Cell Biol.* **31,** 325 (1983).
[5] N. A. Kiselev, E. V. Orlova, V. Ya. Stel'mashchuk, V. D. Vasiliev, O. M. Selivanova, V. P. Kosykh, A. I. Pustovskikh, and V. S. Kirichuk, *J. Mol. Biol.* **169,** 345 (1983).
[6] J. Lake, *J. Mol. Biol.* **161,** 89 (1982).
[7] J. Lake, *J. Mol. Biol.* **105,** 131 (1976).
[8] O. Meisenberger, I. Pilz, M. Stöffler-Meilicke, and G. Stöffler, *Biochim. Biophys. Acta* **781,** 225 (1984).

cant structural features in electron images of isolated biological macromolecules,[9,10] thereby pushing back the frontier of argumentability.

Improving the Signal-to-Noise Ratio of Electron Micrographs

Electron micrographs of macromolecules are noisy due to a number of factors: (1) Biological specimens are extremely sensitive to bombardment by electrons. Radiation-induced structural alterations include evaporation of light atoms, translocation of atoms, and ultimately disintegration. (2) Images are formed by electrons impinging on a photographic emulsion. This "electron counting" process is essentially a Poisson statistical one, with the associated uncertainty being the square root of the number of quanta detected. (3) Heavy atom salts (e.g., uranyl acetate) are commonly used to provide image contrast by negative staining, but the random distribution of stain and the formation of stain crystallites during electron exposure is yet another source of noise.

It is impossible in any experimental situation to eliminate all noise factors at once. Low-dose electron microscopy preserves the specimen, but the recorded images are very noisy since fewer electrons are used to form them. With increasing electron doses, radiation damage increases significantly. Sophisticated techniques such as cryoelectron microscopy can only reduce the rate of destruction by a factor of no more than 10, and also give images with low contrast which are not easily interpreted. Alternative methods of specimen preparation which do not require negative stain, e.g., glucose embedding, also result in low-contrast images. Thus, even under the best possible conditions, the signal-to-noise ratio of electron micrographs will be poor.

An improvement of the signal-to-noise ratio of electron images can be achieved by *a posteriori* image processing. The restoration of noise-degraded images is a topic that has received much attention in many fields.[11] In electron microscopy, the conceptually simplest and most suitable approach to image improvement is that of image averaging.[5,12-16] In a set of many noisy images of an object, the noise at any position varies from

[9] M. van Heel and J. Frank, *Ultramicroscopy* **6,** 187 (1981).
[10] M. van Heel, *Ultramicroscopy* **13,** 165 (1984).
[11] W. K. Pratt, "Digital Image Processing," Wiley, New York, 1978.
[12] D. L. Misell, "Image Analysis, Enhancement, and Interpretation," North-Holland, Amsterdam, 1978.
[13] P. N. T. Unwin and R. Henderson, *J. Mol. Biol.* **94,** 425 (1975).
[14] J. Frank, W. Goldfarb, D. Eisenberg, and T. S. Baker, *Ultramicroscopy* **3,** 283 (1978).
[15] J. Frank, A. Verschoor, and M. Boublik, *Science* **214,** 1353 (1981).
[16] M. van Heel and M. Stöffler-Meilicke, *EMBO J.* **4,** 2389 (1985).

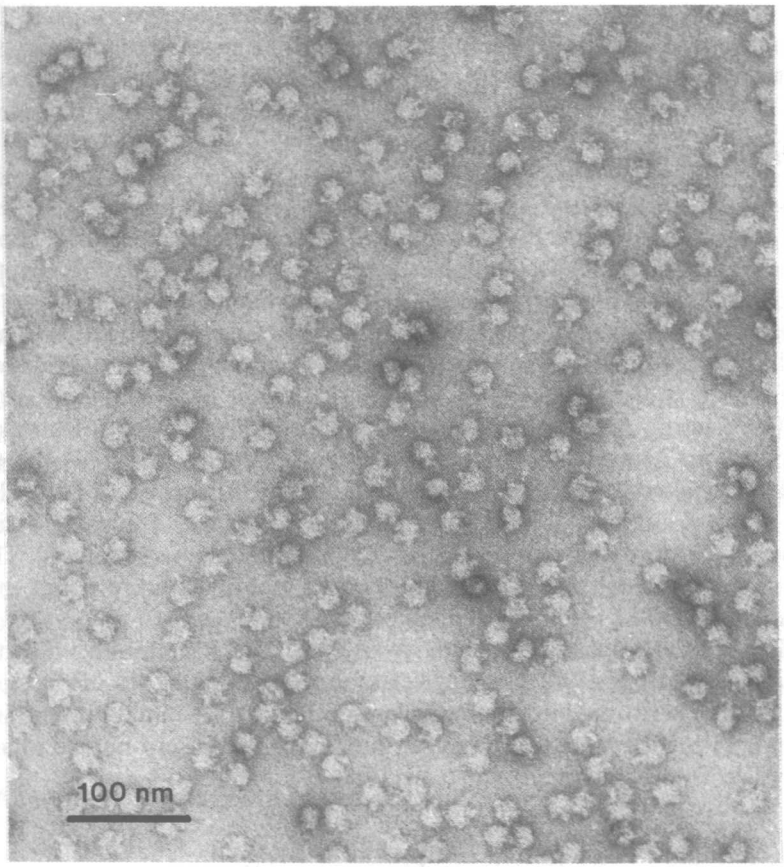

FIG. 1. Electron micrograph of 50S ribosomal subunits.

image to image, but the desired feature information is the same. By averaging together these noisy images, the reproducible signal is enhanced with respect to the random background noise.

In analyzing electron micrographs of isolated biological macromolecules (Fig. 1), there are two problems concerning particle orientation which must first be overcome, since we can only obtain meaningful averages of images that are very similar. First of all, individual particles lie at all angles and positions on the specimen support film and must first be brought into register both rotationally and translationally. Second, biological macromolecules may assume more than one stable position on the support, thus providing essentially different projections through the object. The analysis of mixed populations of images requires the use of multivariate statistical

analysis and classification techniques.[9,10,16] In this chapter, we shall describe the stepwise application of these powerful image-processing tools to electron micrographs of the 50S ribosomal subunit of *Escherichia coli.*

Data Preparation

Isolated 50S subunits were prepared for electron microscopy on a single-layer carbon film by the method of Valentine and negatively contrasted with 1% uranyl acetate.[17] Electron micrographs used in this chapter were taken on a Philips EM 400 at an instrumental magnification of 60,000 and an accelerating voltage of 100 kV. Each specimen area was not preilluminated prior to being micrographed, to minimize the total electron dose.

The electron micrographs were digitized using a Datacopy (Datacopy Corporation, Mountain View, CA) digitizing camera, controlled by an IBM personal computer. This process renders the information on the film into a form suitable for manipulation by a computer. Typically, entire micrographs were digitized in 1728×2240 picture elements (pixels). The scanning step (pixel size) was 32 μm, and so each pixel corresponds to a square area of 0.53 nm size at the object level.

The digitized data were copied to a VAX 11/780 computer (Digital Equipment Corporation) via magnetic tape. There, analyses of digitized images were performed in the framework of the IMAGIC image processing system,[18] which is a general purpose, interactive, and user-oriented image analysis software package.

Selection and Pretreatment of Molecular Projections

A typical electron micrograph is shown in Fig. 1. All distinct particles that were not overlapping or in close contact with other particles were selected interactively from each digitized micrograph using a raster-scan image display system in conjunction with a joystick-controlled cursor.[18] At *least* a few hundred individual molecules must be selected to achieve statistical significance of the results. In this instance, a total of 1956 images were obtained from 15 micrographs. Although at present we do the particle selection interactively, larger populations of molecules can be handled using automated particle selection algorithms.[19,20] At this stage, each indi-

[17] R.C. Valentine, B. M. Shapiro, and E. R. Stadmann, *Biochemistry* **7**, 2143 (1968).
[18] M. van Heel and W. Keegstra, *Ultramicroscopy* **7**, 113 (1981).
[19] M. van Heel, *Ultramicroscopy* **8**, 331 (1982).
[20] J. Frank and T. Wagenknecht, *Ultramicroscopy* **12**, 169 (1984).

vidual macromolecule and its immediate background are represented as a square array of $n \times n$ numbers; n is 72 in this example, but generally n ranges from 48 to 96, depending on the size of the object and the desired resolution.

The many single molecular images must be pretreated by band-pass filtering to suppress the very low and very high spatial frequencies. The very high spatial frequencies represent mostly noise and their contribution can thus be weighted down at this early stage. The very low spatial frequencies also represent unwanted information, e.g., gradual fluctuations in the average densities which depend largely on the amount and uniformity of specimen staining. The frequency limits of band-pass filtering generally vary from specimen to specimen. For our ribosome images, we have determined empirically that a low frequency cutoff of about 13 nm and a high-frequency cutoff of about 1.3 nm are reasonable. Moreover, the low-frequency components (but not the high) are set to a fraction of their original values (typically 1.5%) so that they can be easily restored at a later stage if needed.

After band-pass filtering to enhance only the important structural information, the particles are surrounded by a circular mask to cut away unnecessary background. Finally, the images are standardized by (1) "floating" within this mask to a zero average density, and by (2) multiplication of each pixel by a factor (different for each image) to normalize the variance.[16]

Alignment of Images within the Plane

Isolated macromolecules exhibit a full range of rotational orientations in the plane of the support film. Furthermore, the particle is not yet precisely centered in its image, and a translation in the plane is also required to bring all particles into register. To achieve this registration, we use a computerized alignment algorithm (Fig. 2) based on the use of cross-correlation functions.[21-23]

The alignment process requires first the selection of a reference image with respect to which all other molecular images will be aligned. In the case of the 50S ribosomal subunit, the predominant projection view in electron micrographs is the "crown" view; to a much lesser extent, a "kidney" view is exhibited. Therefore, we choose as an initial reference a well-preserved,

[21] W. O. Saxton and J. Frank, *Ultramicroscopy* **2**, 219 (1977).

[22] J. Frank, *in* "Computer Processing of Electron Microscope Images" (P. W. Hawkes, ed.), p. 187. Springer-Verlag, Berlin, Federal Republic of Germany, 1980.

[23] M. Steinkelberg and H. J. Schramm, *Hoppe-Seyler's Z. Physiol. Chem.* **361**, 1363 (1980).

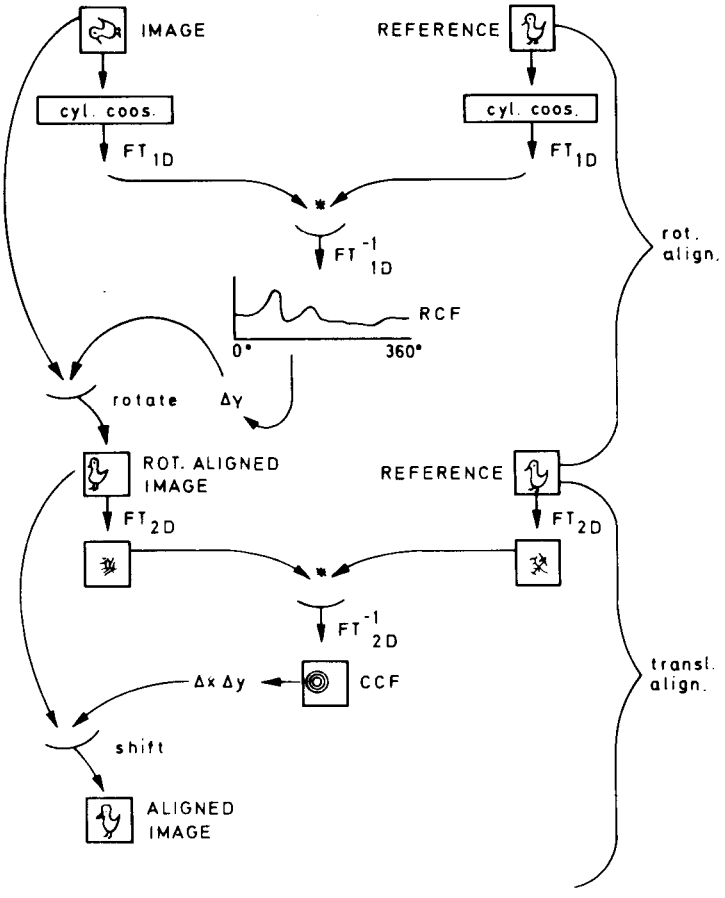

FIG. 2. Schematic of single particle alignment process. Cyl. coos, cylindrical coordinates; FT_{1D}, FT_{2D}, Fourier transform, one-dimensional, two-dimensional; RCF, rotational correlation function; rot. align.; rotational alignment; transl., translational; CCF, cross-correlation function.

canonical crown view (Fig. 3a). The particle is centered within the image, masked by interactive contouring[18] (Fig. 3b) and thresholded within the mask (Fig. 3c) to reduce the effects of any remaining background and of negative stain within the particle.

Rotational alignment between a molecular image and the chosen reference image is achieved by searching for a maximum in the rotational correlation function (RCF). The image and reference are both converted from their usual representation in Cartesian coordinates to one in cylindrical coordinates, and the cylindrical images are then Fourier transformed in

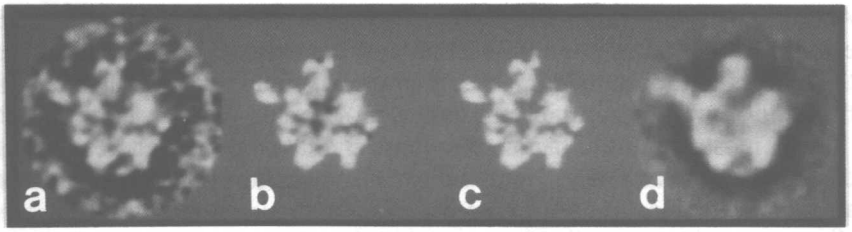

FIG. 3. (a) A single noisy image selected as the initial reference. Dark areas represent stain, while light areas represent protein (or absence of stain). (b) The image in (a) contoured to reduce the effect of the remaining background. (c) The image in (b) thresholded within the contour to reduce the effect of negative stain within the particle. The light areas remaining represent predominantly structural information. (d) An intermediate sum of the 20 images which correlate best with the image in (c); used as a new reference in another alignment in order to refine further alignment parameters.

the tangential direction. The resulting series of one-dimensional Fourier transforms are conjugate multiplied with each other, and the RCF is obtained by integrating the inverse Fourier transform of this product over the radial coordinate. The molecular image is rotated by the angle θ at which the RCF function is found to have its maximum.

Following the rotational alignment, translational alignment is performed by searching for the position of the maximum in the cross-correlation function (CCF). The rotated molecular image and the reference image are Fourier transformed, and the two-dimensional Fourier transforms are conjugate multiplied by each other. The CCF is obtained from this product by inverse Fourier transforming. The rotated molecular image is shifted by $(-\Delta x, -\Delta y)$ to the position of maximum translational overlap. The value of this peak overlap is called the cross-correlation coefficient (CCC).

The sequence of rotational and translational alignment is normally repeated once more to refine the rotation angle and shift parameters.[23]

When the entire data set has been aligned with respect to the initial noisy reference, a smaller set of 20 or so molecular images is selected on the basis of the cross-correlation peak height, i.e., those molecules most similar to the reference after alignment. These selected images are then averaged together to give a better, less noisy reference (Fig. 3d), and the double alignment process is repeated again with the original images and using this new reference.

Refinement of Alignments

This method of aligning images is very sensitive and can deal with noisy images in which the motif may be even more obscured than in Fig. 3a.[21,23]

As with any computational tool, though, it must be carefully applied. For example, the form of band-pass filtering of the data has a strong effect on the success of the alignment. If the alignment is not good, a refinement of the band-pass filter parameters is indicated.

The most important factor affecting the results of an alignment is the choice of reference image. Here, a distinct crown view has been chosen as an initial reference. Since this reference still contains noise, repeating the alignments with "better" references will bring the images into better positions relative to each other. A second reference is therefore made from the average of the 20 or so images that correlate best with this first reference. Clearly, these images will "look like" each other, as will the average. Since we have a great deal of *a priori* knowledge of the low-resolution structure of the ribosome, we have a good idea of the sort of structure we expect to see in the end. However, with a macromolecule of initially unknown structure, it is not clear which projection view is most suitable as an initial reference image and we are faced with a "bootstrapping" problem which can only be solved iteratively. We shall return to this point in the discussion on multi-reference alignment.

Multivariate Statistical Analysis of Mixed Populations

For flat, disklike molecules such as glutamine synthetase[14] (glutamate–ammonia ligase), the two-dimensional alignment process is sufficient to analyze the entire population, since all molecular images have now been brought into a similar orientation. However, most molecules present more than one projection, and thus some means must be developed to determine and extract the predominant and characteristic views.

Multivariate statistical analysis techniques are powerful tools for dealing with mixed populations of macromolecular images.[9,16,24-28] In particular, correspondence analysis (a special form of principal components analysis) is used to extract relevant information from the mixed data set. Each image of $n \times n$ pixels can be thought of as representing a point in $n \times n$ dimensional space, and the entire set of images forms a cloud in this space. Correspondence analysis determines a new, rotated coordinate system in which the first axis represents the direction of greatest interimage variance, the second axis the direction of largest remaining interimage variance, and

[24] J. Frank, A. Verschoor, and M. Boublik, *J. Mol. Biol.* **161,** 107 (1982).
[25] J. Frank and M. van Heel, *J. Mol. Biol.* **161,** 134 (1982).
[26] M. M. C. Bijlholt, M. van Heel, and E. F. J. van Bruggen, *J. Mol. Biol.* **161,** 139 (1982).
[27] J. Frank and A. Verschoor, *J. Mol. Biol.* **178,** 696 (1984).
[28] A. Verschoor, J. Frank, and M. Boublik, *J. Ultrastruct. Res.* **92,** 180 (1985).

so on. The cloud of images can now be described with respect to this new coordinate system. More precisely, each of the aligned images can be expressed as a linear combination of the predominant, independent eigenimages extracted from the set (Fig. 4a). The first eigenimage (with chi-squared metrics) points at the center of mass of the full data set. Subsequent eigenimages describe decreasing amounts of the interimage variance

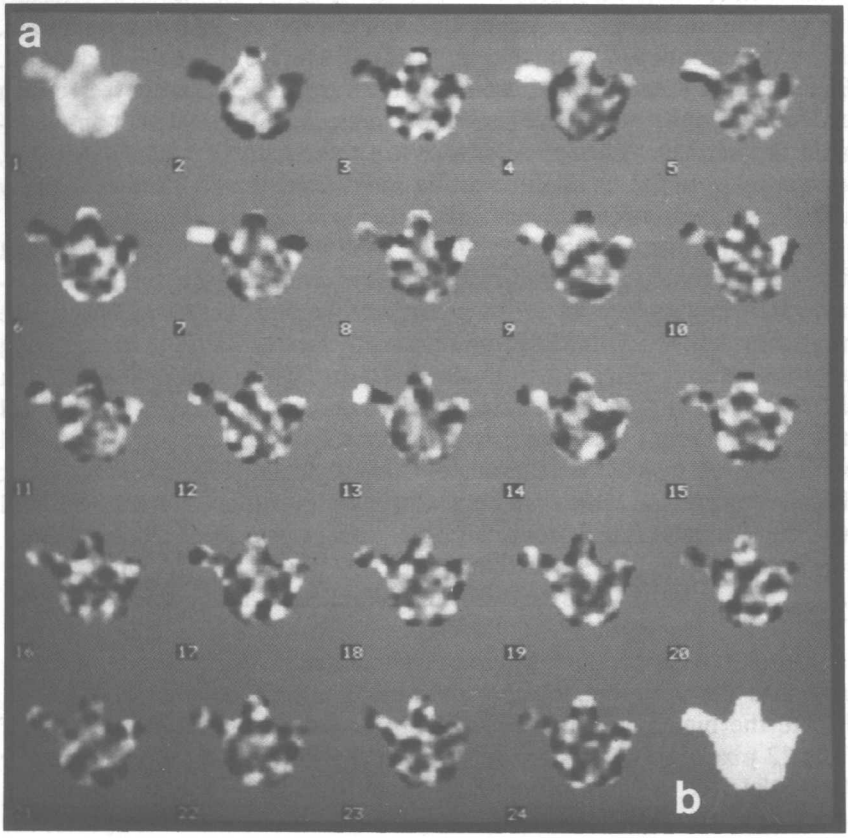

FIG. 4. (a) The data set of 1956 aligned images is decomposed by correspondence analysis into eigenimages which represent the principal components of interimage variation. The first eigenimage points to the center of mass of the full data set. The second, third, fourth, and fifth eigenimages describe 6.2, 4.9, 1.9, 1.7, and 1.4% of the total interimage variance, respectively, whereas the twenty-fourth eigenimage describes only 0.8%. All 24 eigenimages account for 34.2% of the total interimage variance. (b) Binary mask generated from the total sum of 1956 aligned images, defining the image area active in correspondence analysis. The total sum is a blurry image which indicates those regions within the image area within which the pixels belong (usually) to the molecule and not to negative stain or carbon support film.

of the data set, and in our case soon represent predominantly noise. By disregarding these higher order components, and only considering the significant ones (typically of the order of 6 to 24), the images can be considered as points in a much smaller (than $n \times n$) dimensional space. We have thus achieved a very large reduction in the amount of data to be analyzed as well as a significant amelioration of the effect of noise.

The eigenimages of Fig. 4a can often be interpreted in terms of structural features that they describe. The lower order eigenimages typically comprise lower spatial frequency information than the higher order ones. The first eigenimage points to the overall average of the full data set. Eigenimage 2 describes predominantly the shape difference between crown and kidney views, while eigenimage 3 represents internal density modulations. Eigenimage 4 has strong density in the region of the L7/L12 stalk, indicating presence or absence of the stalk. Eigenimage 5 seems to show that the stalk can move up and down.

Before performing correspondence analysis, the aligned images must first be pretreated to mask off image areas not representing relevant structural information.[26,27] In other words, we want to compare only those image areas in which the 50S subunit usually lies, and not the surrounding negative stain in which it is embedded. To do this, a mask is formed from the sum of all of the aligned molecules. The region of interest is contoured interactively using a display program,[18] and a mask image is generated containing 1s inside the contour and 0s outside it (Fig. 4b). This mask defines those pixels which are active during correspondence analysis, and which ultimately contribute to the classification statistics.

Classification

The data compression achieved by correspondence analysis in turn facilitates the grouping together of those images that are most similar, despite the high noise present in them. In our example, each image of 72×72 pixels is at this stage represented by only 24 components rather than 5184. We use an automatic hierarchical classification algorithm[10] in which similar images are initially merged together to form classes; these are themselves grouped further together to form larger and larger classes until finally one class containing all of the images is obtained. The classification procedure is usually stopped, however, when a predetermined number of classes (typically from 30 to 60) is obtained. (The number of final classes is chosen so that each class contains of the order of 30 to 40 members.) This partitioning is indicated with the 50S subunit because this particle assumes a relatively small number of positions on the support film, and we would like to find these positions regardless of their relative occurrence.[10]

During the classification, about 15% of the aligned population is initially rejected (on the basis of their large variance contribution) as representing either misaligned molecules or uncharacteristic images which appear rarely. There are also some "bad" classes which have a high internal variance; either they have few members, or their members are poorly aligned. These classes, too, are discarded. Of most interest in subsequent analyses are the "good" classes, composed of images which are most similar to each other. The aligned images in each class are summed together to give an "average" image with an enhanced signal-to-noise ratio. In these sums, sources of random noise such as variations in the stain distribution around the molecules, radiation-induced structural alterations, and variations in the background carbon support film are averaged out and become less significant compared to the common signal. The class averages thus represent the most commonly occurring projection views with high statistical significance, and indicate directions which we must explore further.

In our example of the *E. coli* 50S subunit, the two-dimensional map of factorial coordinate 2 versus coordinate 3 (Fig. 5) suggests a rough decomposition of the data set into three major groups. Individual class sums representative of each group are shown in Fig. 6. We interpret these as representing different projections of the subunit: two types of crown views and one type of kidney view. One of the differences between the two crown views is the form of the the bulge on the right-hand side of the particle (the L1 protuberance). This is already a significant result, since previously we were not able to distinguish these subtle differences in the original noisy images. However, the map also indicates that there may be a continuous transition between these extremes, and the hierarchical ascendant classification algorithm elucidated some other minor class averages in addition to the major ones. By this stage, we have some knowledge of the extent and type of heterogeneity in the input data.

Multireference Alignment

In the next step of the analysis, a number of class averages (generally from 2 to 12, but 8 in this example) from the data set are selected and used as references, along with their mirror views, in a new set of alignments. These new references are less noisy than the original ones, and this results in a better alignment. Moreover, the new references represent trends in the data set which we want to explore. These trends are due to interparticle variability in specific structural features as well as to the different positions of the macromolecule on the support film. Mirroring the references elimi-

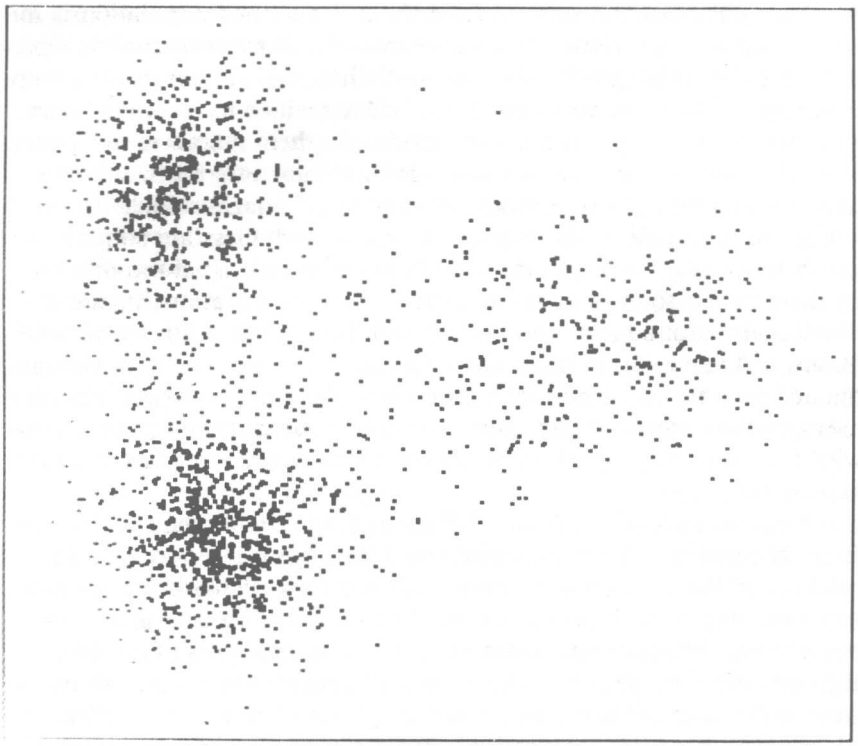

FIG. 5. Correspondence analysis map of factorial coordinates 3 (vertical axis) versus 2 (horizontal axis). Each image is represented as a dot, and the entire population forms a cloud. There are two major subpopulations, blending into a more diffuse third group.

nates bias in the alignment: the particle usually has only one preferred face of attachment to the support, but may occasionally lie on its other side.

In multireference alignment, each macromolecular image is aligned with respect to *each* new reference in turn. The CCC is a measure both of the goodness of alignment and of the noisy macromolecule's similarity to

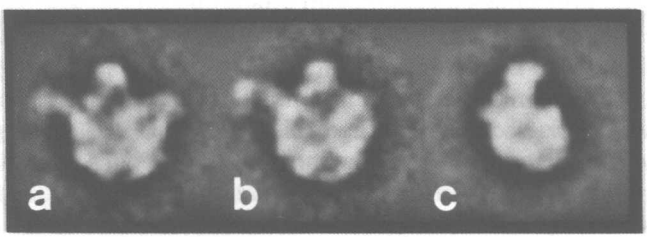

FIG. 6. Classes representative of the three groups seen on the correspondence analysis map.

the particular reference. The alignment parameters giving the highest CCC are the ones finally used to rotate and shift this particular image. The final data set is now better aligned because the reference images are less noisy and are also varied, consistent with the heterogeneity of the input images. The newly aligned data set can now undergo correspondence analysis and classification again. The class sums obtained after this refinement step are the ones finally studied in detail.

Figure 7 shows some of the final class sums of the 50S subunit, selected

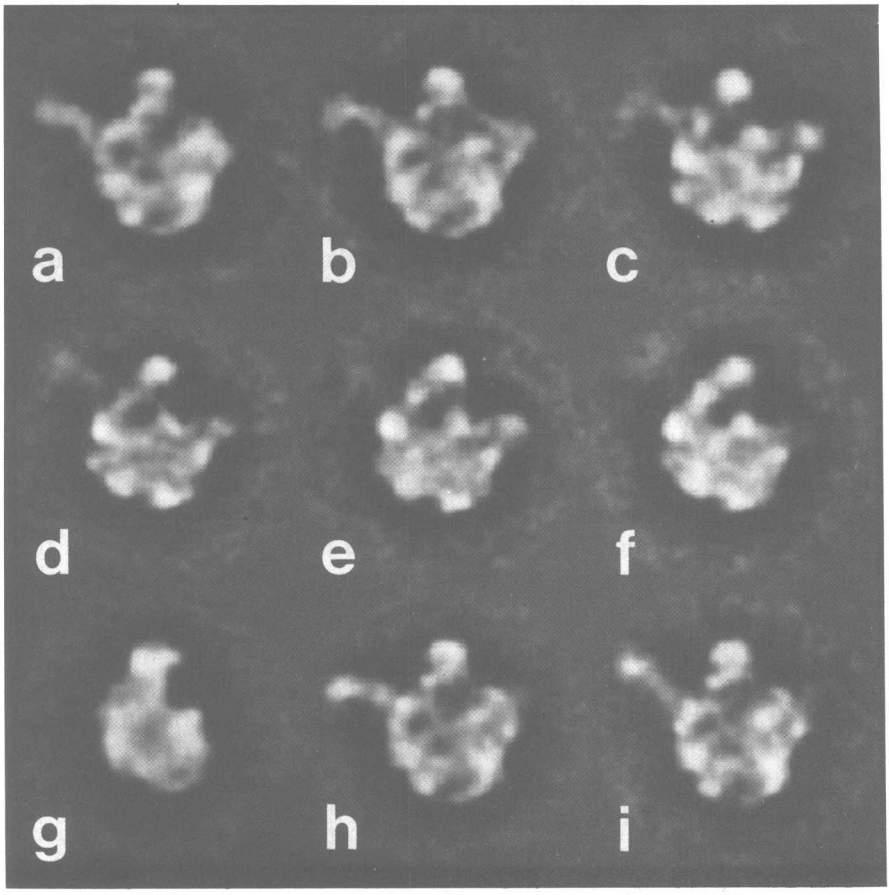

FIG. 7. Partitioning of the population of 1956 images into classes; those with a low intraclass variance are selected for final analysis. The two crown views (a and b) are predominant (forming about two-thirds of the classes). The remaining classes appear to be views intermediate between the crown and kidney (c–g). In the final two crown classes (h and i), the L7/L12 stalk lies in different positions, spanning a distance of over 2 nm.

on the basis of low intraclass variance and representing the varied characteristic views of the 50S subunit in this population. Previous studies based solely on visual interpretation have defined only two main views, namely, crown and kidney. Our statistical analysis of a large number of particles shows that more views may exist in this electron microscopical preparation. The two types of crown views are the most commonly occurring (about two-thirds of the population), but to a lesser extent we also have kidney views and other views of the subunit appearing to lie in slightly different positions on the support film. The series of seven class sums (Fig. 7a–g) show the 50S subunit apparently rotating from the crown to the kidney view; the L7/L12 stalk gradually becomes weaker in density and eventually disappears, while the L1 protuberance (on the right-hand side) and the notch between it and the central protuberance become progressively more pronounced. Interestingly, there are no pairs of classes which are mirror views of each other.

The sensitivity of correspondence analysis is exemplified by the subtle difference between two crown class averages (Fig. 7h and i) which differ only in the position of the flexible L7/L12 stalk. This flexibility, as well as the variability of the L1 protuberance, have been subjects of previous and independent studies[6,7,28] and are important to keep in mind when attempting to understand the three-dimensional structure of the 50S subunit. At this stage, however, the computational work is over and we must now revert to our own (human) interpretational abilities to decide whether interclass differences are due to flexibility of structural features or to different positions of the macromolecule on the support film. A more detailed biological analysis will thus appear elsewhere.

Visually, the quality of the class averages is much better than of the original images. Objectively, the reproducible resolution between two pairs of similar classes is typically 2.2 to 2.4 nm, determined by the Fourier ring correlation method.[16] Between any two original images of a class, the reproducible resolution is about 6 nm, indicating the significant improvement achieved by image averaging.

Concluding Remarks

The information content of electron micrographs can be enhanced significantly by *a posteriori* image processing. We have described and demonstrated powerful techniques for analyzing noisy electron images of isolated macromolecules. The fundamental principle underlying each step of the analysis is the reduction of the effect of noise, whether by band-pass filtering, principal components analysis, or averaging similar images to provide better references for alignment. This approach has allowed us to

determine objectively both flexibility of certain structural features and the potential existence of numerous distinct projection views in normal electron microscopical preparations of the *E. coli* 50S ribosomal subunit. With direct three-dimensional reconstruction techniques,[29-33] these projections can be used to obtain the three-dimensional structure of the subunit.

Acknowledgments

We thank Professor H. G. Wittmann and Mr. H. Gewitz of the Max-Planck-Institut for Molecular Genetics for the 50S ribosomal subunits, and Professor E. Zeitler for comments on the manuscript. George Harauz was the recipient of a Postdoctoral Fellowship from the Medical Research Council of Canada.

[29] G. Harauz and F. P. Ottensmeyer, *Ultramicroscopy* **12,** 309 (1984).
[30] A. Verschoor, J. Frank, M. Radermacher, T. Wagenknecht, and M. Boublik, *J. Mol. Biol.* **178,** 677 (1984).
[31] G. Harauz and M. van Heel, *in* "Pattern Recognition in Practice" (E. S. Gelsema and L. N. Kanal, eds.), Vol. 2, p. 279. North-Holland, Amsterdam, 1986.
[32] G. Harauz and M. van Heel, *Optik* **73,** 146 (1986).
[33] M. van Heel, *Ultramicroscopy* **21,** 111 (1987).

[3] Structural Analysis of Ribosomes by Scanning Transmission Electron Microscopy

By MILOSLAV BOUBLIK, GERRIT T. OOSTERGETEL, VALSAN MANDIYAN, JAMES F. HAINFELD, and JOSEPH S. WALL

The potential of high-resolution transmission electron microscopy (TEM) for the determination of the morphology of ribosomes and topographical mapping of their components and functional sites has been demonstrated elsewhere in this volume [4]. This chapter focuses on those features of dark-field scanning transmission electron microscopy (STEM) which make this technique uniquely suited to the quantitative structural analysis of ribosomes and other sensitive biological specimens.[1] The major advantage of the dedicated STEM is the separation of the components that affect resolution and contrast (Fig. 1). The probe-forming components (field emission gun, condenser lens, aperture, deflection coils, and objective lens) are all above the specimen, leaving the space below the specimen free for optimization of detectors (annular detectors for elastic scattering,

[1] J. S. Wall, *in* "Introduction to Analytical Electron Microscopy" (J. J. Hren, J. I. Goldstein, and D. C. Joy, eds.), pp. 333-342. Plenum, New York, 1979.